Global Journal of Engineering Innovations & Interdisciplinary Research

Review Article

Cobalt-Cerium Oxide Supported Zeolite Film Catalyst for Enhancing CO Oxidation

Dong Zhang[1,*], Hai Ming Sha[2], Joe R Zhao[1], Helen J Sun[1], Brian J Cao[1]

[1]Tri-Y Environmental Research, 2655 Lillooet St., Vancouver, B.C., Canada V5M 4P7

[2]Nanjing Hydraulic Research Institute, No. 223, Guangzhou Road, Nanjing, P. R. China 210029

Correspondence

Dr. Dong Zhang

Tri-Y Environmental Research, 2655 Lillooet St., Vancouver, B.C., Canada V5M 4P7.

- Received Date: 22 Sep 2024
- Accepted Date: 04 Nov 2024
- Publication Date: 09 Nov 2024

Keywords

Cobalt-Cerium; CO oxidation; Structured catalyst; Zeolite

Abstract

Co-Ce/NaA zeolite film/metal fiber catalysts were synthesized for the oxidation of low-concentration carbon monoxide. The support was prepared via in-situ hydrothermal synthesis, and cobalt and cerium oxide were added through incipient wetness impregnation. Parameters like Co/Ce ratio, metal loading, and calcination temperature were optimized. A catalyst with 24 wt% Co and 6 wt% Ce loading, calcined at 500°C for 2 hours, showed the best performance and stability. Both fresh and used catalysts were analyzed using H2-TPR, XRD, Nitrogen isotherms, SEM, EDS mapping, and XPS. The results indicated a partial transition of cobalt oxide to an amorphous state during the stability test.

Introduction

The protracted exposure to minor concentrations of carbon monoxide (CO) in enclosed areas such as submarines, spacecraft, and indoor parking structures can result in chronic poisoning. One of the most effective methodologies for mitigating CO is catalytic oxidation. Though noble metals such as platinum, gold, and rhodium exhibit exceptional catalytic activity, their exorbitant cost and limited availability inhibit their large-scale deployment. Consequently, there has been an increasing focus on transition metal oxides such as copper, iron, manganese, and particularly cobalt-based catalysts, which are not only abundant but also resistant to deactivation by poisoning. Cobalt oxide catalysts have proven promising in a wide array of reactions, including CO oxidation. Moreover, the inclusion of cerium oxide operates as a beneficial additive, offering a substantial oxygen storage capacity linked with the rapid Ce4+/Ce3+ redox process. This process facilitates an increased availability of oxygen for the oxidation procedure, thereby enhancing the catalytic activity. Co-Ce catalysts exhibit high activity in various reactions including CO and Volatile Organic Compounds (VOCs) oxidation, methane combustion, Fischer-Tropsch synthesis, among others.

Zeolites are considered ideal substrates for catalysts due to their extensive specific surface area, homogeneous pore structure, and presence of acid sites. Numerous types of zeolites such as BEA[1, 2], FAU[3], MOR[4-7], MFI[8-10], CHA[11,12] and LTA[13, 14] have been previously employed as catalyst supports. Among these, LTA zeolites present a certain appeal due to their selectivity and superior thermal stability. They have demonstrated excellent performance in applications including Volatile Organic Compounds (VOCs) combustion and CO oxidation.[15-17] However, the use of granule and powder catalysts faces certain limitations due to high mass and heat transfer resistance, significant bed pressure drop, and low contacting efficiency. Contrastingly, zeolite film supports are considered more advantageous than these granular supports, displaying marked enhancements such as high mass and heat transfer rates, reduced bed pressure drop, and increased contacting efficiency.[18]

The objective of the present study is threefold: firstly, to synthesize Co-Ce catalysts supported on LTA (4A) zeolite film/metal fiber; secondly, to optimize the Co/Ce ratio, total metal loading, and calcination temperature for CO oxidation, and thirdly, to evaluate the stability of the catalysts post a 48-hour operation period.

Experimental

Materials

3-Aminopropyltrimethoxysilane (APTMS) (> 97%, Aladdin Industrial Corporation); Sodium hydroxide (> 96%, Nanjing Chemical Reagent Co., Ltd); Sodium aluminate (Al2O3 >41%); LUDOX HS-30 colloidal silica (30% SiO2/water, Aldrich); Toluene (99.5%, Hunan Hengyang Kaixin Chemical Co., Ltd); Co(NO3)3·6H2O (99.0%, Tianjin Kermel Reagent Co., Ltd); Ce(NO3)3·6H2O (99.0%, Tianjin Kermel Reagent Co., Ltd); Stainless

Citation: Zhang D, Sha HM, Zhao JR, Sun HJ, Cao BJ. Cobalt-Cerium Oxide Supported Zeolite Film Catalyst for Enhancing CO Oxidation. Japan J Res. 2024;1(1):02

steel fibers (6.5 μm in diameter, Huitong Advanced Materials Co., Ltd); NaA zeolite (250-425 μm in diameter, Pingxiang Xintao Zeolite Co., Ltd); CO/Air mixture (180 ppm, Guangzhou Zhuozheng Air Co., Ltd).

Preparation of catalysts

The innovative porous NaA zeolite film/metal fiber composites, comprised of metal fibers were fabricated through the application of a wet lay-up mixing process succeeded by in-situ hydrothermal synthesis, in accordance with the previously reported methodology.[19] The Co-Ce modified NaA zeolite film/metal fiber catalysts were subsequently prepared via the process of incipient wetness impregnation. The impregnating medium consisted of a solution containing $Co(NO_3)_3$ and $Ce(NO_3)_3$ at predetermined Co and Ce concentrations.

The samples underwent impregnation at a controlled temperature of 298K for a duration of 12 hours, followed by a drying phase at 423K for 4 hours, and finally calcination in an air environment at a specified temperature for 2 hours. The nomenclature adopted for the catalysts was CoxCey-aC, where 'x' and 'y' denote the respective Co and Ce loadings, and 'a' represents the calcination temperature (°C). The granular Co-Ce catalysts were designated with the appended suffix '-Granule'. Furthermore, the unused and utilized catalysts subsequent to the stability test were marked with the suffixes '-Fresh' and '-Used' respectively.

Characterization

H_2-Temperature Programmed Reduction (H2-TPR) examinations were conducted on a Quantachrome Automated Chemisorption Analyzer by subjecting the sample to heat in a H_2/Air (10 vol%) atmosphere at a heating rate of 10°C·min-1 in the range of 100 to 700°C. X-ray diffraction (XRD) patterns were generated on a D8 Advance (manufactured by Bruker Co.) diffractometer employing Cu Kα radiation (set at 40 kV, 40 mA). The specific surface area and pore size distribution were determined via an ASAP 2020 Analyzer (manufactured by Micromeritics Instrument Co., Ltd) at a temperature of 77K. The samples were degassed at 250°C for a duration of 4 hours under vacuum conditions.

Morphological analysis and elemental distribution assessments were conducted with the aid of Scanning Electron Microscopy (SEM, model Hitachi S-3700N), with Elemental Mapping performed by Energy Dispersive Spectroscopy (EDS mapping, model Quantax, produced by Bruker Co.) in conjunction with the microscope chamber. X-ray Photoelectron Spectra (XPS) data were acquired via a Kratos Axis Ultra (DLD) spectrometer utilizing Al Kα (1486.6 eV) radiation. The Binding energies for Co 2p, Ce 3d, and O 1s were calibrated with reference to the C 1s signal (284.5 eV) from carbon impurity.

Catalytic test

Catalytic activity evaluations were conducted within a continuous-flow fixed bed reactor, comprised of a stainless-steel tube (with an internal diameter of 10 mm and a length of 450 mm), under standard atmospheric pressure. The reactor's temperature was supervised using E-type thermocouples. A feed, composed of 180 ppm CO balanced with Air, was channeled through the reactor with a bed height of 10 mm at a rate of 100 mL·min-1. The Gas Hourly Space Velocity (GHSV) was established at 7643 h-1.

The outlet concentration of CO was monitored using an infrared gas analyzer (model QGS-08B, manufactured by Baif-Maihak Co.). The CO conversion was computed in alignment with the following equation:

$$C_{CO} = \frac{CO_{in} - CO_{out}}{CO_{in}} \times 100\%$$

where Cco was the CO conversion, Coin and COout represented the inlet and outlet CO concentration.

Results and discussion

Effects of Co/Ce ratio

The influence of the Co/Ce ratio was scrutinized by varying this ratio within the spectrum of 30:0 to 0:30, while the total metal loading remained constant at 30 wt%. The catalysts were calcined at a temperature of 500°C.

Subsequently, these catalysts were characterized by H2-TPR to elucidate the redox properties, as depicted in Fig. 1. For the majority of the catalysts containing cobalt, two consecutive reduction peaks between 200 and 400°C were discerned. These peaks, termed α and β respectively, can be attributed to the stepwise reduction of cobalt oxide. The α peak is associated with the reduction of Co3+ ions, which exist within the spinel structure (Equation 1), while the β peak results from the reduction of CoO to metallic cobalt (Equation 2).[20, 21] In certain samples (namely, Co18Ce12-500C and Co6Ce24-500C), the α peaks were challenging to distinguish, as they overlapped with the β peaks. The pure CeO2 sample (Co0Ce30-500C) displayed a reduction peak around 460°C, attributable to the removal of surface capping oxygen ions during the reduction process. [22, 23] . The reduction peak associated with the bulk oxygen of CeO2 was anticipated around 800°C, but this is beyond the detectable temperature range.[24]

$$Co_3O_4 + H_2 = 3CoO + H_2O \quad (1)$$

$$CoO + H_2 = Co + H_2O \quad (2)$$

The α and β peaks of Co30Ce0-500C were at 294 and 323°C, while the peaks of most samples with the addition of cerium oxide, shifted to lower temperature. For example, the α peak of Co24Ce6-500C is at 255°C; the β peak of Co18Ce12-500C is at 305°C. This may be caused by the interaction of cobalt oxide and cerium oxide. According to the report elsewhere, the higher dispersion could contribute to the lower reduction temperature peak in TPR analysis.[25] Therefore, the samples with lower reduction temperature such as Co24Ce6-500C is likely to have the higher dispersion of cobalt oxide, which leads to the higher catalytic activity.

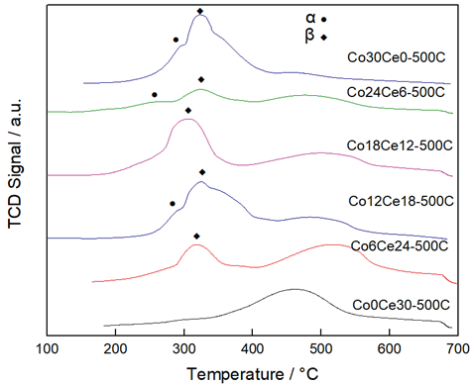

Figure 1. *TPR profiles of catalysts of different Co/Ce ratio.*

The catalytic efficacy of catalysts with varying Co/Ce ratios has been assessed, as depicted in Fig. 2. This implies that overall catalytic activities exhibit a volcanic curve as the Co/Ce ratio escalated from 0:30 to 30:0. Among the samples, Co18Ce12-500C and Co24Ce6-500C demonstrated the most pronounced activity towards CO oxidation. Conversely, the sample devoid of cobalt — Co0Ce30-500C — displayed suboptimal performance due to the absence of active cobalt oxide species. The superior performance of Co18Ce12-500C and Co24Ce6-500C can be attributed to the heightened dispersion of cobalt oxide, as corroborated by TPR results. Additionally, the incorporation of CeO2 enhanced oxygen storage capacity, further facilitating the oxidation process.[24]

In comparison with Co18Ce12-500C, Co24Ce6-500C performed marginally better as it exhibited enhanced activity at lower (80°C) and higher (>110°C) temperatures. Consequently, Co24Ce6-500C was selected as the benchmark for subsequent investigations.

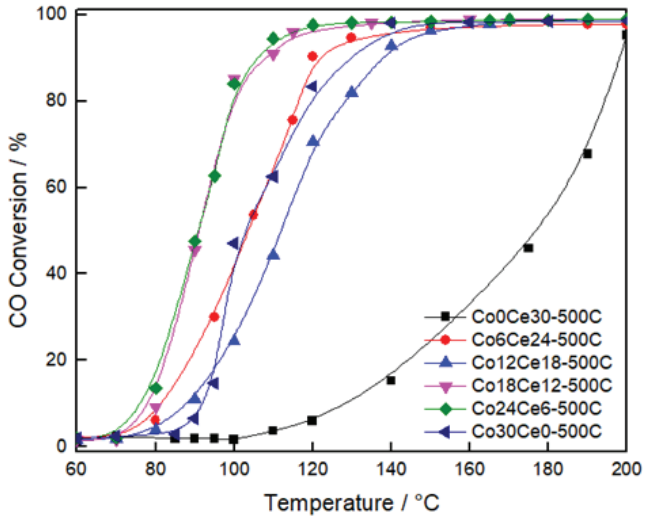

Figure 2. *Catalytic activity of catalysts of different Co/Ce ratio.*

Effects of total metal loading

The impact of total metal loading was probed while maintaining the Co/Ce ratio at a constant 4 and altering the metal loading between 20 to 40 wt%. The catalysts were calcined at a temperature of 500°C. Fig. 3 delineates the H2-TPR profiles of these catalysts. Generally, as total metal loading amplifies, the α and β peaks become more pronounced, indicating a higher amount of cobalt oxide. Nevertheless, the α peak is no longer discernible in Co32Ce8-500C, possibly due to its overlap with the β peak. Furthermore, the reduction temperature of α and β peaks in Co24Ce6-500C is the lowest among all, indicating the cobalt oxide on this catalyst boasts the highest dispersion. The α peak in Co24Ce6-500C is more intense than in other samples, representing a substantial amount of highly dispersed cobalt oxide. This property could prove beneficial to catalytic activity. Additionally, the reduction peaks observed around 500°C are ascribed to the cerium oxide, as previously discussed.

Figure 4 illustrates the catalytic activities of catalysts with differing total metal loadings. Co24Ce6-500C and Co32Ce8-500C exhibit nearly identical activity while Co16Ce4-500C presents inferior performance. The heightened activity of Co24Ce6-500C is due to the high dispersion of cobalt oxide.

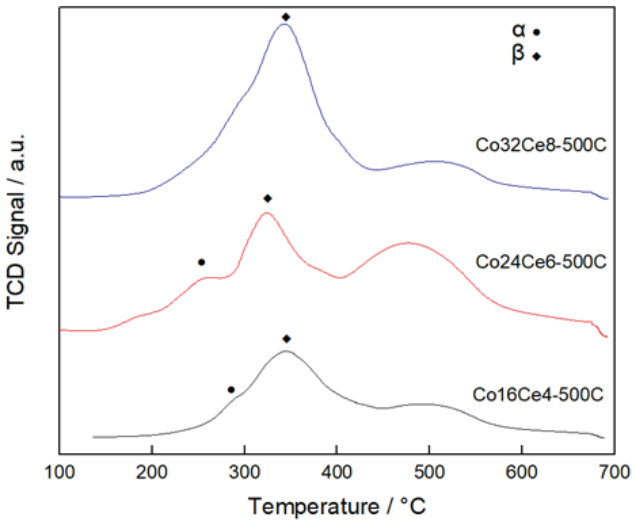

Figure 3. *TPR profiles of catalysts of different total metal loading.*

However, as the metal loading incrementally increased from 30 to 40 wt%, the activity did not improve. A substantial amount of metal oxide on the surface caused aggregation rather than a highly dispersed state of cobalt oxide. Conversely, the large content of cobalt and cerium oxide offset the loss of highly dispersed cobalt oxide. As a result, catalytic activity did not enhance with an increase in total metal loading. Even though Co24Ce6-500C and Co32Ce8-500C exhibited similar activity, Co24Ce6-500C was preferred due to its lower metal loading which translates to reduced costs. Therefore, it was chosen as the benchmark for further study of calcination temperature.

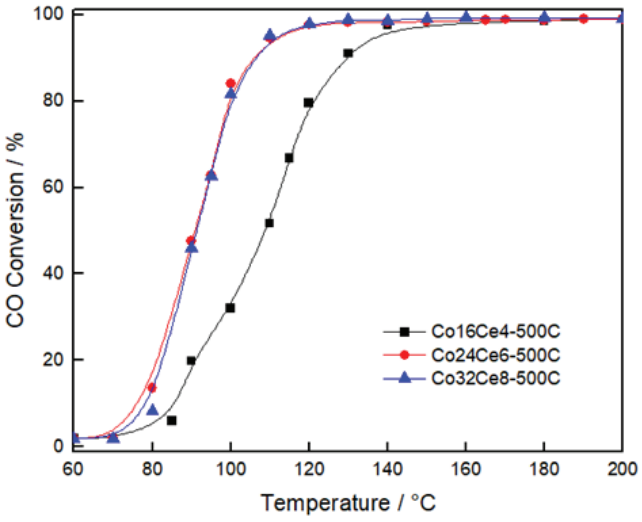

Figure 4. *Catalytic activity of catalysts of different total metal loading.*

Although Co24Ce6-500C and Co32Ce8-500C had the similar activity, Co24Ce6-500C was preferred because of the less metal loading which led to the low cost. Therefore, it was selected as the reference for further study of calcination temperature.

Effects of calcination temperature

The influence of calcination temperature was assessed by varying the calcination temperature from 400 to 600°C. All catalysts were laden with 24 wt% Co and 6 wt% Ce.

Figure 5 showcases the H2-TPR profiles of the catalysts. Except for Co24Ce6-600C, both α and β peaks can be identified. For Co24Ce6-400C, the reduction temperature corresponding to α and β peaks was 283 and 370°C, respectively, which is greater than that of Cu24Ce6-500C (255 and 325°C). This implies that the redox ability of Cu24Ce6-400C is inferior to that of Cu24Ce6-500C. Furthermore, the absence of the α peak in Cu24Ce6-600C suggests it was overlapped by the β peak, suggesting the α peak in this sample must exist at a higher temperature, signifying lower reduction ability. Thus, we can infer that the calcination temperature significantly impacts the redox ability of catalysts by manipulating the combinational state between cobalt and cerium oxide.

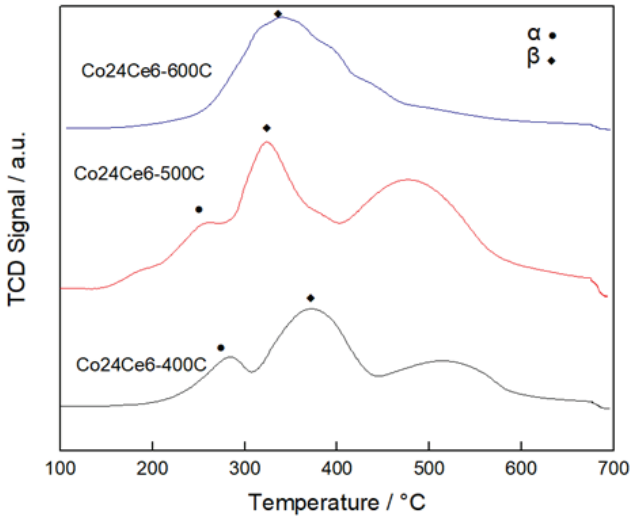

Figure 5. *TPR profiles of catalysts of different calcination temperature.*

The catalytic efficacy of catalysts calcinated at disparate temperatures has been investigated, as shown in Fig. 6. Co24Ce6-600C exhibited the poorest performance. Concurrently, Co24Ce6-500C and Co24Ce6-400C displayed analogous activity at lower temperatures (<100°C), but at higher temperatures (>100°C), Co24Ce6-500C demonstrated superior performance. The substandard activity of Co24Ce6-600C can be attributed to the fact that the redox ability of the catalyst was constrained. As seen in the TPR profile, the unobservable α peak at higher temperature is a consequence of a low dispersion state brought about by the elevated calcination temperature. This suggests that the aggregation of metal clusters of low catalytic activity could have been generated, thus accounting for the poor performance of Co24Ce6-600C. Regarding Co24Ce6-400C, it manifested diminished performance at higher temperatures, also attributable to the lower dispersion state of cobalt oxide, as indicated by TPR, where both α and β peaks were shifted to higher temperatures. Therefore, after optimization of synthetic factors, it can be concluded that the catalysts with 24 wt% Co and 6 wt% Ce calcinated at 500°C for 2h exhibit the best catalytic activity.

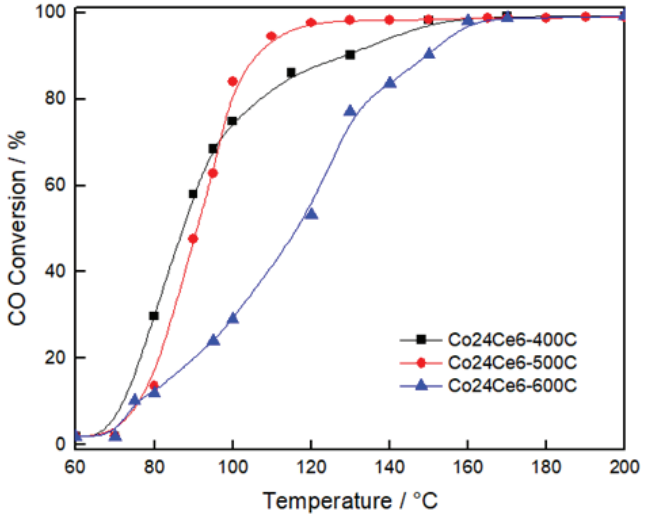

Figure 6: *Catalytic activity of catalysts of different calcination temperature.*

Catalytic performance of catalysts with different supports

To illustrate the impact of the NaA zeolite film/metal fiber, we also evaluated the catalytic performance of the Co-Ce/NaA zeolite film/metal fiber composite (also known as Co24Ce6-500C), Co-Ce/metal fiber catalyst (without the zeolite film), and granular Co-Ce/NaA zeolite catalyst (250-425 μm in diameter). All catalysts were loaded with 24 wt% Co and 6 wt% Ce and calcinated at 500°C. The results are depicted in Fig. 7. The catalytic performance of the Co-Ce/NaA zeolite film/metal fiber catalyst significantly surpasses that of the Co-Ce/metal fiber catalyst and granular Co-Ce zeolite catalyst. The potential reason why the Co-Ce/NaA zeolite film/metal fiber catalyst outperforms the granular Co-Ce/NaA zeolite catalyst is that the structured metal fiber support provides relatively lower mass transfer resistance. As such, internal diffusion resistance can be largely eliminated, and the contacting efficiency can thus be amplified.[26] Compared with the Co-Ce/metal fiber, the catalytic activity of the Co-Ce/NaA zeolite film/metal fiber catalyst was also enhanced due to the presence of the zeolite film. The NaA zeolite film offers a relatively large surface area and pore volume to anchor and distribute the active metal species, allowing the cobalt and cerium oxide species to be uniformly distributed, leading to heightened activity.[27].

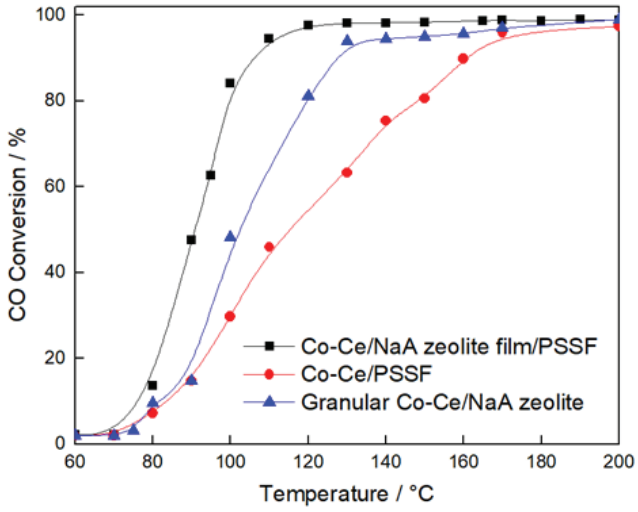

Figure 7. *Catalytic activity of catalysts with different supports.*

Stability test

The stability test for CO oxidation over Co24Ce6-500C was conducted. As shown in Fig. 8, this catalyst displayed impressive stability for CO oxidation. The CO conversion of 98% was maintained for 48h. The fresh and used catalysts, post-stability tests, were further analyzed using H2-TPR, N2 adsorption/desorption isotherms, XRD, XPS, SEM, and EDS mapping.

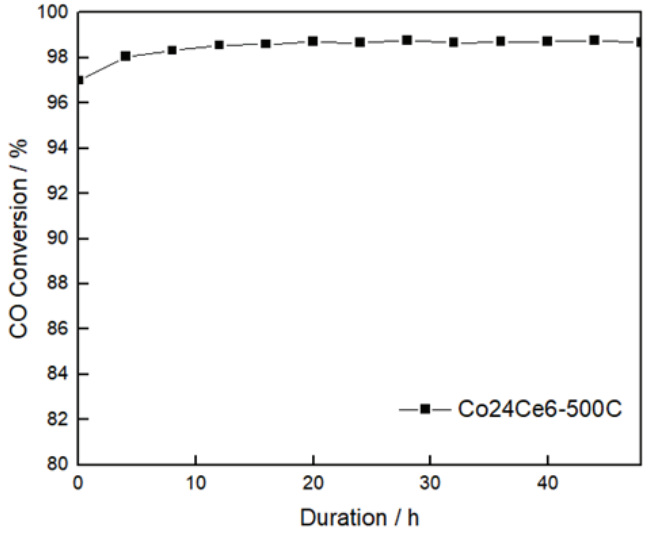

Figure 8. *Stability test for CO oxidation over Co24Ce6-500C (180 ppm CO/Air in the inlet, reaction temperature of 110°C, reaction duration of 48h, GHSV of 7643 h^{-1})*

Figure 9 discloses the H2-TPR profiles of the fresh and used catalysts following the stability test. Both α and β peaks can be observed in both catalysts. Post-stability test, the α peak shifted from 255 to 265°C, while the β peak shifted from 305 to 330°C. This shift could possibly be attributed to the reduction of some cobalt oxide species during the stability test. [28] It could also be due to the minor compromise of the redox ability during the stability test, despite it showing high activity during the stability test.

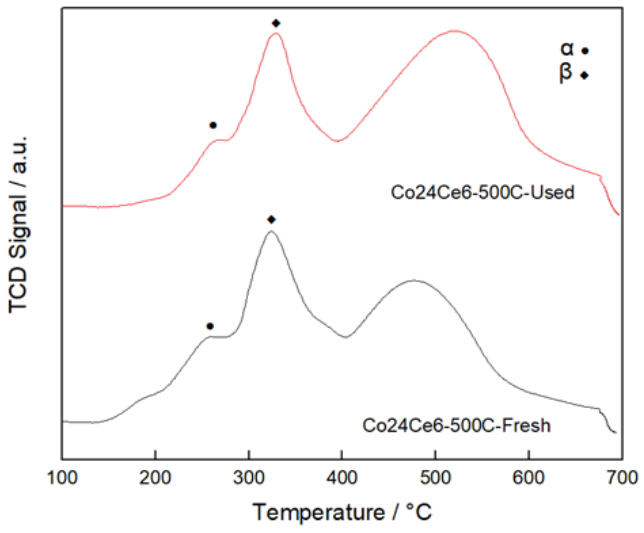

Figure 9. *H2-TPR profiles of the fresh and used catalysts after stability test.*

The textural properties were characterized using N2 adsorption/desorption isotherms, shown in Fig. 10. The pore volume and the BET surface area for the fresh and used catalysts are given in Table 1. As can be seen in Fig. 10, both catalysts barely absorb nitrogen at the lower pressure range (P/P0 = 0 ~ 0.3), not due to the blockage caused by the introduction of metal oxide species, but due to the poor adsorption of N2 molecule at the pore openings of 4A zeolite.[19] The used catalyst exhibited a relatively large mesopore volume, identifiable by the larger hysteresis loop at higher relative pressure. This can also be seen in the detailed data in Table 1. The BET surface area of the fresh catalyst was 24.2 m2·g-1, while that of the used one was 26.7 m2·g-1. Likewise, the mesopore volume slightly increased from 0.109 to 0.114 cm3·g-1. Generally, the relatively higher BET surface area and larger mesopore volume is a result of the slight change in pore structure during CO oxidation.

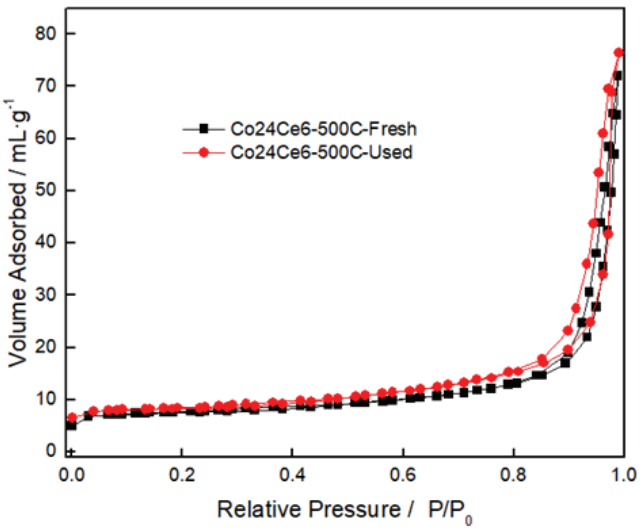

Figure 10. *N2 adsorption/desorption isotherms of the fresh and used catalysts after stability test.*

Table 1. *Pore properties of the fresh and used catalysts after stability test.*

Sample	Pore structure properties			
	Micropore ($cm^3 \cdot g^{-1}$)	Mesopore ($cm^3 \cdot g^{-1}$)	Total volume ($cm^3 \cdot g^{-1}$)	BET Surface area ($cm^3 \cdot g^{-1}$)
Co24Ce6-500C-Fresh	0.007	0.10	0.11	23
Co24Ce6-500C-Used	0.01	0.13	0.14	42

Figure 11 exhibits the XRD patterns of the fresh and used catalysts. Two peaks at 46 and 51° correspond to the support. However, the intensity of these peaks was much weaker than the ones of support as previously reported.[19] Also, the diffraction peaks of NaA zeolite were nearly unobservable in both catalysts. This was likely due to the uniform coverage of the surface by the metal oxide species, making the zeolite layer and substrate difficult to detect by XRD. Additionally, the diffraction peaks related to CeO2 with fluorite structure (2θ = 28, 33, 47°) can be seen in both catalysts.[29] The peaks associated with Co3O4 with spinel structure (2θ = 38, 45°) were visible in the fresh

catalyst. The weakened peaks of Co3O4 were due to the lower crystallinity, which might result from the decrease in crystal size or the transformation to amorphous forms during the stability test.

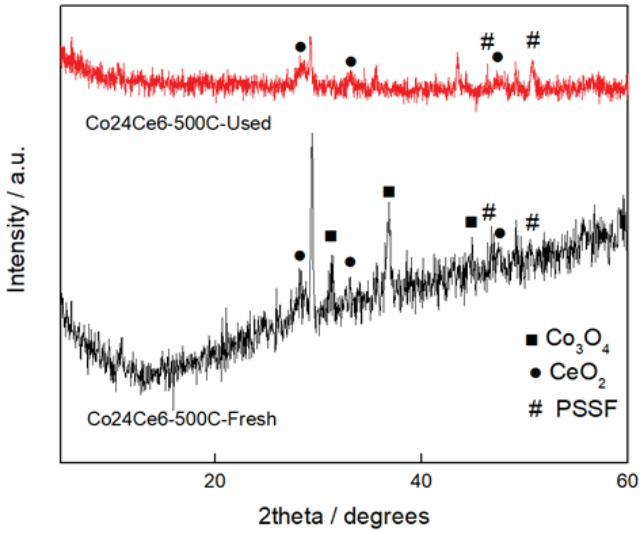

Figure 11. *XRD patterns of the fresh and used catalysts after stability test.*

The SEM was used to characterize the morphology and crystallinity of catalysts, as depicted in Fig. 12. Fig. 12(a) displayed that the junctions of metal fibers were sintered together, forming a 3-D network structure of high mechanical strength. In addition, the metal oxide species were also uniformly covered on the surface. Fig. 12(b) shows the cubic LTA crystals well intergrown on the substrate surface. The thickness of the zeolite layer was about 2 μm according to Fig. 12(c). For the used catalyst, some amorphous species appeared on the surface, as shown in the red circle in Fig. 12(e). Furthermore, a higher number of amorphous species can be identified in Fig. 12(f). It is hypothesized that these amorphous species are related to the cobalt oxide, which aligns with the XRD results that diffraction peaks of Co3O4 were absent for the used catalyst.

The energy-dispersive X-ray spectroscopy mapping (EDS mapping) results in Fig. 13 reveal that both catalysts contained Al, Si, Ce, and Co atoms. The Al and Si elements originated

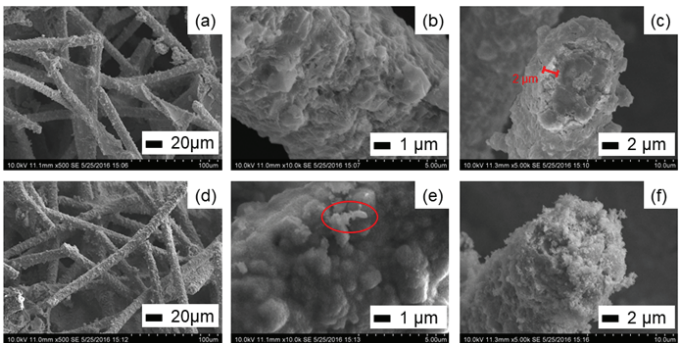

Figure 12. *SEM images of Co24Ce6-500C-Fresh at 500 x (a), 10k x (b) and its intersection at 5k x (c); Co24Ce6-500C-Used at 500 x (d), 10k x (e) and its intersection at 5k x (f).*

from the NaA zeolite film. Both Co and Ce atoms were randomly dispersed on the surface. It can also be observed that the Ce elements were enriched on the surface as evidenced by the green dots distributed in both graphs, despite accounting for only 6 wt% in both catalysts. This observation correlates with the XRD results, showing that diffraction peaks of CeO2 were relatively intense. According to Bao[30], Ce2O3 was also enriched on the surface of Fe2O3-CeO2 catalysts but no explanation was provided.

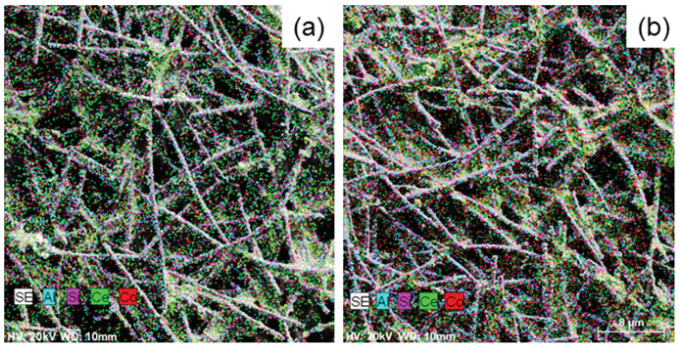

Figure 13. *EDS elemental mapping of Co24Ce6-500C-Fresh (a) and Co24Ce6-500C-Used (b).*

It can be seen in Fig. 14 that XPS spectra of the fresh and used catalysts were very similar, characterized by the presence of the dominant peaks correspondence with the specific elements. The XPS spectra of the survey, Co 2p, Ce 3d and O 1s were presented. In Fig. 14(a), Ce, Co, O and C can be identified. As for the spectra of Co 2p of both catalysts, two broad peaks appeared at 775~783 and 790~798 eV, which were related to Co 2p3/2 and Co 2p1/2. The peak of Co 2p3/2 can be deconvoluted to two peaks at 778.5 and 781.0 eV, which were assigned to Co3+ and Co2+ species, respectively. Similarly, the one of Co 2p1/2 can also be deconvoluted to two peaks at 794.3 and 796.3 eV, which were attributed to Co3+ and Co2+ species.[26] The Ce 3d spectra were illustrated in Fig. 14(c). The peaks related to Ce 3d3/2 and Ce 3d5/2 have been labeled as u and v. The peaks of v, v2, v3, u and u2 were the different Ce 4f electron configurations in the final state of Ce4+ species. Meanwhile, the v1 and u1 can be ascribed to two possible electron configurations of the final state of Ce3+ species.[31, 32] As for the spectra of O 1s, the peak at lower binding energy (528.3 eV) was a characteristic of the lattice oxygen and the one at higher binding energy (530.5 eV) was a result of adsorbed oxygen. [26] The adsorbed oxygen was likely due to the oxygen vacancies on cerium oxide. It has been known that the presence of oxygen vacancies is important for the catalytic application.[29]

Conclusion

The Co-Ce/NaA zeolite film/metal fiber catalysts were successfully synthesized using in-situ hydrothermal synthesis followed by incipient wetness impregnation. The catalyst composed of 24 wt % Co and 6 wt% Ce and calcined at 500°C for 2 hours exhibited the best activity. This catalyst was further compared with the Co-Ce of the same metal loading supported on metal fiber or granular zeolite. The findings indicated that the Co-Ce/NaA zeolite film/metal fiber catalyst was superior. Impressively, this catalyst maintained a CO conversion of 98% at 110°C for 48 hours, indicative of its high stability. The

characterization results suggested that the textual properties of the catalysts were nearly unchanged after the stability test, except for the cobalt oxide on the surface, which partially transformed into an amorphous form.

Conflict of Interest (COI) Statement

The authors declare that they have no known competing financial interests or personal relationships that could have appeared to influence the work reported in this manuscript. All authors have approved the final version of the manuscript and agree with its submission to the Journal.

Data availability statement

The datasets generated and/or analyzed during the current study are available from the corresponding author on reasonable request.

References

1. Wei S, Dai H, Long J, et al. Chemical Engineering Journal. 2023;455:140726. doi:10.1016/j.cej.2022.140726.
2. Jeevapong W, Sittiwong J, Probst M, et al. The Journal of Physical Chemistry C. 2023;127(18):8473-8481. doi:10.1021/acs.jpcc.3c01170.
3. Yin J, Xia D, Sun H, et al. Molecular Simulation. 2023;49(1):36-59. doi:10.1080/08927022.2022.2123947.
4. Park JW, Kim SJ, Seo M, et al. Appl Catal A. 2008;349(1–2):76-85. doi:10.1016/j.apcata.2008.07.006.
5. Zhang X, Shen Q, He C, et al. Catal Sci Technol. 2012;2(5):1059-1067. doi:10.1039/C2CY00445C.
6. Pérez NC, Miró EE, Zamaro JM. Catal Today. 2013;213:183-191. doi:10.1016/j.cattod.2013.02.014.
7. He H, Miao C, Guo H, Hua W, Yue Y, Gao Z. Reaction Kinetics, Mechanisms and Catalysis. 2022;135(4):2045-2058. doi:10.1007/s11144-022-02231-9.
8. Chen H, Zhang H, Yan Y. Chemical Engineering Journal. 2012;209:372-378. doi:10.1016/j.cej.2012.08.020.
9. Qi G, Yang RT. Appl Catal B. 2005;60(1-2):13-22. doi:10.1016/j.apcatb.2005.01.012.
10. Boroń P, Chmielarz L, Gurgul J, et al. Microporous Mesoporous Mater. 2015;203:73-85. doi:10.1016/j.micromeso.2014.10.023.
11. Leistner K, Mihai O, Wijayanti K, et al. Catal Today. 2015;258:49-55. doi:10.1016/j.cattod.2015.04.004.
12. Zhang D, Yang RT. Appl Catal A. 2017;543:247-256. doi:10.1016/j.apcata.2017.06.021.
13. Sun T, Wei J, Zhou C, et al. International Journal of Hydrogen Energy. 2023;48(37):13851-13863. doi:10.1016/j.ijhydene.2022.12.288.
14. Yoshida Y, Sada Y, Sano T, Okubo T, Wakihara T. Crystal Growth & Design. 2023;23(4):2231-2238. doi:10.1021/acs.cgd.2c01277.
15. Ohgushi T, Ishimaru K, Komarneni S. J Am Ceram Soc. 2001;84(2):321-327. doi:10.1111/j.1151-2916.2001.tb00657.x.
16. Rosso I, Galletti C, Saracco G, Garrone E, Specchia V. Appl Catal B. 2004;48(3):195-203. doi:10.1016/j.apcatb.2003.10.016.
17. Zhou C, Zhang H, Yan Y, Zhang X. Microporous Mesoporous Mater. 2017;248:139-148. doi:10.1016/j.micromeso.2017.04.020.
18. Chen H, Zhang H, Yan Y. Industrial & Engineering Chemistry Research. 2012;51(51):16643-16650.
19. Zhang D, Zhang H, Yan Y. RSC Adv. 2015;5(68):54913-54919. doi:10.1039/C5RA07380D.
20. Tang CW, Kuo MC, Lin CJ, Wang CB, Chien SH. Catal Today. 2008;131(1):520-525. doi:10.1016/j.cattod.2007.10.026.
21. Wang J, Shen M, Wang J, et al. Catal Today. 2011;175(1):65-71. doi:10.1016/j.cattod.2011.03.004.
22. Rao GR, Sahu HR, Mishra BG. Colloids Surf A Physicochem Eng Asp. 2003;220(1):261-269. doi:10.1016/S0927-7757(03)00080-3.
23. Zheng X, Wang S, Wang X, Wu S. Mater Lett. 2005;59(22):2769-2773. doi:10.1016/j.matlet.2005.04.025.
24. Zou G, Xu Y, Wang S, Chen M, Shangguan W. Catal Sci Technol. 2015;5(2):1084-1092. doi:10.1039/C4CY01141D.
25. Dow WP, Wang YP, Huang TJ. J Catal. 1996;160(2):155-170. doi:10.1006/jcat.1996.0135.
26. Yan Y, Wang L, Zhang H. Chemical Engineering Journal. 2014;255:195-204. doi:10.1016/j.cej.2014.05.141.
27. Yuranov I, Renken A, Kiwi-Minsker L. Appl Catal A Gen. 2005;281(1-2):55-60. doi:10.1016/j.apcata.2004.11.012.
28. Chen H, Yan Y, Shao Y, Zhang H. RSC Adv. 2014;4(98):55202-55209. doi:10.1039/C4RA08769K.
29. Todorova S, Kadinov G, Tenchev K, et al. Catal Lett. 2009;129(1):149-155. doi:10.1007/s10562-008-9805-x.
30. Bao H, Chen X, Fang J, Jiang Z, Huang W. Catal Lett. 2008;125(1):160-167. doi:10.1007/s10562-008-9540-3.
31. Bin F, Wei X, Li B, Hui KS. Appl Catal B. 2015;162:282-288. doi:10.1016/j.apcatb.2014.07.007.
32. Katta L, Sudarsanam P, Thrimurthulu G, Reddy BM. Appl Catal B. 2010;101(1-2):101-108. doi:10.1016/j.apcatb.2010.09.012.